

Phase Space of Tokamak Edge Turbulence, the L - H Transition, and the Formation of the Edge Pedestal

B. N. Rogers and J. F. Drake

Institute for Plasma Research, University of Maryland, College Park, Maryland 20742

A. Zeiler

Max-Planck-Institut für Plasmaphysik, EURATOM Association, 85748 Garching, Germany

(Received 3 April 1998; revised manuscript received 22 June 1998)

Based on three-dimensional simulations of the Braginskii equations, we identify two main parameters which control transport in the edge of tokamaks: the MHD ballooning parameter and a diamagnetic parameter. The space defined by these parameters delineates regions where typical L -mode levels of transport arise, where the transport is catastrophically large (density limit) and where the plasma spontaneously forms a transport barrier (H mode). [S0031-9007(98)07608-X]

PACS numbers: 52.55.Fa, 52.25.Fi, 52.30.Jb, 52.35.Ra

The tokamak edge region, comprising the transition zone from the inner, hot core plasma to the outer, cold scrape-off layer, exerts vital control over the plasma discharge through its role in the L - H (low-high confinement) transition [1,2], the density limit [3], and the edge temperature pedestal. We claim here, based on three-dimensional simulations of the Braginskii equations, that these phenomena are fundamentally linked to the dependence of the turbulent edge transport on two dimensionless parameters: the MHD ballooning parameter $\alpha = -Rq^2 d\beta/dr$ and a diamagnetic parameter α_d (defined below). The space spanned by these parameters is shown in Fig. 1. In the weak diamagnetic limit (small α_d), the simulations show a dramatic rise in the transport with increasing α that leads to high transport levels even at small α values well below the limit of ideal ballooning instability [4,5]. We associate this behavior with an effective density limit beyond which stable tokamak operation is not possible. At higher $\alpha_d \sim 1$, on the other hand, the α dependence of the turbulence is reversed, with small but finite values of α leading to a strong suppression of transport. In this regime a local increase in the

pressure gradient, above a threshold in α , causes a *reduction* of the transport. Since such a reduction would naturally lead to a further steepening of the edge pressure gradient, this region of higher α and α_d is unstable to the spontaneous formation of a transport barrier. The boundary of this unstable domain defines the onset condition for the L - H transition in our model. Finally, the global stability of the edge pedestal and the relative roles of finite α and $\mathbf{E} \times \mathbf{B}$ shear are explored in dynamical simulations of the barrier formation process. These simulations confirm that the $\mathbf{E} \times \mathbf{B}$ shear effect can stabilize turbulence during the formation of the barrier [6,7]. We also find, however, that, for small α , the $\mathbf{E} \times \mathbf{B}$ shear alone is not sufficient to trigger a transition due to the strong positive dependence of transport on the plasma pressure gradient.

The simulations are carried out in a poloidally and radially localized, flux-tube domain that winds around the torus [8]. Assuming a shifted-circle magnetic geometry, the nonlinear equations for perturbations of the magnetic flux $\tilde{\psi}$, electric potential $\tilde{\phi}$, density \tilde{n} , electron and ion temperatures \tilde{T}_e , \tilde{T}_i , and parallel flow \tilde{v}_{\parallel} are

$$\hat{\alpha}[\partial_t \tilde{\psi} + \alpha_d \partial_y \tilde{\psi}(1 + 1.71\eta_e)] - \nabla_{\parallel}[\tilde{\phi} - \alpha_d(\tilde{p}_e + 0.71\tilde{T}_e)] = \tilde{J}, \quad (1)$$

$$\nabla_{\perp} \cdot d_t \nabla_{\perp}(\tilde{\phi} + \tau \alpha_d \tilde{p}_i) + \hat{C}(\tilde{p} + \tilde{G}) - \nabla_{\parallel} \tilde{J} = 0, \quad (2)$$

$$d_t \tilde{n} + \partial_y \tilde{\phi} = \tilde{F}, \quad \tilde{F} = \epsilon_n \hat{C}(\tilde{\phi} - \alpha_d \tilde{p}_e) - \epsilon_v \nabla_{\parallel} \tilde{v}_{\parallel} + \alpha_d \epsilon_n (1 + \tau) \nabla_{\parallel} \tilde{J}, \quad (3)$$

$$d_t \tilde{T}_i + \eta_i \partial_y \tilde{\phi} = \frac{2}{3} [\tilde{F} + \frac{5}{2} \epsilon_n \tau \alpha_d \hat{C} \tilde{T}_i + \kappa_i \nabla_{\parallel} (\nabla_{\parallel} \tilde{T}_i + \hat{\alpha} \eta_i \partial_y \tilde{\psi})], \quad (4)$$

$$d_t \tilde{T}_e + \eta_e \partial_y \tilde{\phi} = \frac{2}{3} [\tilde{F} - \frac{5}{2} \epsilon_n \alpha_d \hat{C} \tilde{T}_e + 0.71 \alpha_d \epsilon_n (1 + \tau) \nabla_{\parallel} \tilde{J} + \kappa_e \nabla_{\parallel} (\nabla_{\parallel} \tilde{T}_e + \hat{\alpha} \eta_e \partial_y \tilde{\psi})], \quad (5)$$

$$d_t \tilde{v}_{\parallel} = -\epsilon_v [\nabla_{\parallel}(\tilde{p} + 4\tilde{G}) + (2\pi)^2 \alpha \partial_y \tilde{\psi}], \quad (6)$$

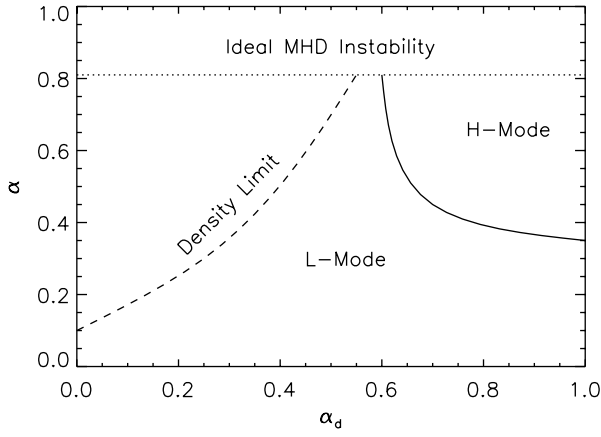
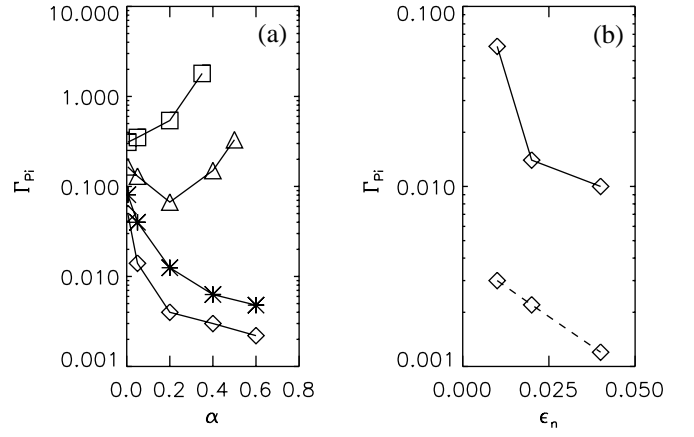


FIG. 1. Edge plasma phase space.

where $\nabla_{\parallel} = \partial_z + \hat{\alpha} \hat{z} \times \nabla_{\perp} \tilde{\psi} \cdot \nabla_{\perp}$, $d_t = \partial_t + \hat{z} \times \nabla_{\perp} \tilde{\phi} \cdot \nabla_{\perp}$, $\nabla_{\perp}^2 = [\partial_x + \Lambda(z) \partial_y]^2 + \partial_y^2$, $\hat{C} = [\cos(2\pi z) + \Lambda(z) \sin(2\pi z) - \epsilon] \partial_y + \sin(2\pi z) \partial_x$, $\Lambda(z) = 2\pi \hat{s} z - \alpha \sin(2\pi z)$, $\tilde{G} = 2\gamma_p [\hat{C}(\tilde{\phi} + \tau \alpha_d \tilde{p}_i) - 4(\epsilon_v / \epsilon_n) \nabla_{\parallel} \tilde{v}_{\parallel}]$, $\tilde{J} = \nabla_{\perp}^2 \tilde{\psi}$, $\tilde{p}_{\alpha} = \tilde{n} + \tilde{T}_{\alpha}$, $\tilde{p} = (\tilde{p}_e + \tau \tilde{p}_i) / (1 + \tau)$. The time (t), perpendicular (x, y), and parallel (z) normalization scales are $t_0 = (RL_n/2)^{1/2}/c_s$, $L_0 = L_z [C^2 \eta_{\parallel} / (4\pi v_A^2 t_0)]^{1/2}$, and $L_z = 2\pi q_a R$. The diamagnetic and MHD parameters are $\alpha_d = \rho_s c_s t_0 / [(1 + \tau) L_n L_0]$, $\alpha = q_a^2 R \beta / L_p$. Other parameters are $\tau = T_{i0} / T_{e0}$, $\eta_{\alpha} = L_n / L_{T_{\alpha}}$, $\epsilon = a/R$, $\epsilon_n = 2L_n/R$, $\epsilon_v = \epsilon_n^{1/2} / (4\pi q_a)$, $\hat{\alpha} = (2\pi)^2 \alpha L_p / L_n$, $L_n / L_p = [1 + \eta_e + \tau(1 + \eta_i)] / (1 + \tau)$, $\kappa_e = 1.6\alpha_d^2 \epsilon_n (1 + \tau)$, $\kappa_i = 0.064(m_p/m_i)^{1/2} \tau^{5/2} \alpha_d^2 \epsilon_n (1 + \tau)$, $\gamma_p = 0.16\pi^2 q_a^2 \kappa_i$. The parallel coordinate values $z = 0$ and $z = \pm 1/2$ represent the outboard and inboard midplanes, respectively. The transverse flux coordinates x, y correspond to local radial and poloidal variables. Unless noted otherwise, we consider the values $\hat{s} = 1$, $\tau = 1$, $\epsilon_n = 0.02$, $\epsilon = 0.2$, $q_a = 3$, $\eta_i = \eta_e = 1$, and $m_i/m_p = 2$.

The application of a fluid model to tokamak edge discharges is reasonable because the mean-free path of electrons λ_e is typically smaller than the connection length L_z . For parameters at the L - H transition in the case of ASDEX-U [9], for example, $\lambda_e/L_z < 0.05$ ($R = 165$ cm, $a = 50$ cm, $B = 2.5$ T, $T_e = 100$ eV, $n \sim 3 \times 10^{13}$ cm $^{-3}$, $Z_{\text{eff}} = 2$, $q = 4$). Further, since $v_{*i,e} \gg 1$ (in the ASDEX-U example, $v_{*e} > 20$), trapped particles should not play a major role. Finally, the dominant modes in our simulations satisfy $k_{\perp} \rho_i \ll 1$.

Figure 2(a) shows the normalized, poloidally averaged ion energy flux $\Gamma_{pi} \approx -\langle \tilde{p}_i \tilde{\phi}_y \rangle$ versus α for various values of α_d . For small $\alpha_d < 0.5$ the transport increases strongly with increasing α , while for larger $\alpha_d \sim 1$, the transport at higher α is suppressed. This reversal reflects the fact that the turbulence in the small and large α_d cases is driven by different mechanisms with contrary dependences on electromagnetic effects.

FIG. 2. (a) $\Gamma_{pi}(\alpha)$ for $\alpha_d = 0.25$ (squares); $\alpha_d = 0.5$ (triangles); $\alpha_d = 0.75$ (asterisks); $\alpha_d = 1$ (diamonds); (b) $\Gamma_{pi}(\epsilon_n)$ for $\alpha_d = 1$ and $\alpha = 0.05$ (solid line); $\alpha = 0.6$ (dashed line).

In the small α_d case, the turbulence results mainly from the nonlinear development of resistive ballooning modes [8]. The enhancement of the transport at higher α in this case is due to the dependence of the turbulence on magnetic field perturbations [4]. For very small $\alpha_d \lesssim 0.3$ the transport becomes extremely large even at small $\alpha \sim 0.3$. The evolution of the edge into this regime would lead to a large flux of plasma from the core into the edge and a possible radiation collapse. Since $\alpha_d \propto T/\sqrt{n}$ while $\alpha \propto nT$, the limit of small α_d and finite α is consistent with larger n and smaller T , and in Fig. 1 we label the rough boundary of this forbidden zone as a “density limit.” In agreement with this, the edge discharge parameters at the density limit in ASDEX-U are similar to those given previously, aside from a lower temperature ($T_e = 50$ eV) [9], with corresponding values of $\alpha_d \sim 0.3$ and $\alpha \sim 0.5$. The energy diffusion rate predicted by the simulations for these parameters is immense: $D = \Gamma_{pi} D_0$ with $D_0 = L_0^2/t_0 \sim 60$ m 2 /s and [see Fig. 2(a)] $\Gamma_{pi} \sim 1$. This picture is also consistent with observations on Alcator-C that confinement degrades as the density limit is approached [3].

In the case $\alpha_d \sim 1$, resistive ballooning modes are weakened by diamagnetic effects [8], and the turbulence is predominantly caused by a nonlinear electron drift wave instability [8,10]. This instability relies on the nonlinear production of poloidal pressure gradients, which (unlike radial gradients) excite unstable drift waves even in the presence of the equilibrium magnetic shear [10]. The drift waves grow due to the convection of the electron pressure across the magnetic field, which generates a parallel pressure gradient $\nabla_{\parallel} p_e$ and an associated parallel current through Ohm’s law. This process, however, is inhibited by electromagnetic effects at very small α . This is because the electrons at higher α convect the magnetic field together with the electron pressure, leading to a large reduction of $\nabla_{\parallel} p_e$ relative to the electrostatic, $\alpha = 0$ limit. This effect can be illustrated by a linear analysis

of a constant ambient density gradient in the y direction $n = n_0 y$. The resulting drift wave growth rate $\gamma_r(k_\perp)$ is shown in Fig. 3 for various values of α (we take $\alpha_d n_0' = 1$, $k_\parallel = 2\pi\hat{s}$, $\tau = 1$, $\eta_{i,e} = 0$, $\epsilon_n = 0$). The strong suppression with increasing α is consistent with Fig. 2(a). A similar effect was invoked in Ref. [11].

To estimate the level of α at which the suppression occurs, note from Eq. (1) that the magnetic perturbations become important in our normalized units when $(2\pi)^2 \alpha \partial_t \sim \nabla_\perp^2$, or with $\partial_t \sim \omega_{*e} \sim \alpha_d k_\perp$, $\alpha \sim k_\perp / [\alpha_d (2\pi)^2]$. To obtain k_\perp , note that the vorticity equation (2) implies $\partial_t \nabla_\perp^2 \tilde{\phi} \sim \alpha_d k_\perp^3 \tilde{\phi} \sim \nabla_\parallel \tilde{J}$, or with $\tilde{J} \sim \nabla_\parallel \tilde{\phi}$ (from Ohm's law) and $\nabla_\parallel \sim 2\pi\hat{s}$ (the inverse shear length), $k_\perp \sim (2\pi\hat{s})^{2/3} \alpha_d^{-1/3}$. As a result, electromagnetic effects become important for $\alpha \sim \hat{s}^{2/3} (2\pi\alpha_d)^{-4/3} \sim 0.1$ (given $\alpha_d \sim 1$, $\hat{s} \sim 1$), consistent with Figs. 2(a) and 3.

Returning to the issue of transport barrier formation, in a stable system an increased pressure gradient leads to enhanced flux, which in turn acts to flatten the gradient. The gradient therefore evolves to a state in which the energy flux and the sources balance. A transport barrier can form spontaneously if the flux *decreases* with increasing gradient. In dimensional units the particle flux (comparable to Γ_{p_i}) can be written as $\Gamma = (D_0 n_0 / L_n) \Gamma_n(\alpha_d, \alpha, \epsilon_n, \dots)$. The dependence on the gradient enters explicitly through the scale length L_n , as well as implicitly through the L_n dependence of D_0 , α_d , α , etc. Excluding the variation of Γ_n , the flux has a strong positive power dependence $\Gamma \sim n_0'^2$. The dependence of Γ_n on n' must therefore reverse this for the system to be unstable to the formation of a barrier. This dependence, neglecting the weak variation of $\alpha_d \sim n'^{1/4}$, appears mainly through $\alpha \sim n'$ and $\epsilon_n \sim n'^{-1}$. For small α_d , Γ_n is insensitive to ϵ_n and increases sharply with α [see Fig. 2(a)], which reinforces the stability of the system. No barrier formation is therefore possible for small α_d .

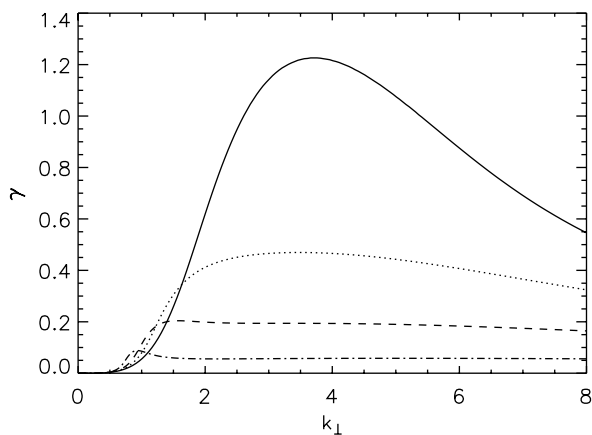


FIG. 3. $\gamma(k_\perp)$ for $\alpha = 0$ (solid line); $\alpha = 0.15$ (dotted line); $\alpha = 0.3$ (dashed line); $\alpha = 0.6$ (dot-dashed line).

At higher $\alpha_d \sim 1$, on the other hand, the α dependence of $\Gamma_{p_i}(\sim \Gamma_n)$ shown in Fig. 2(a) is reversed, allowing the possibility that $d\Gamma_n/d|n'|$ could change sign. The suppression with increasing α in this case must compete with the n'^2 dependence of the normalization, as well as a strong destabilizing trend due to decreasing $\epsilon_n = 2L_n/R$ [8]—see Fig. 2(b). To determine the net dependence on the scale length, simulations were carried out in the range $\epsilon_n \sim 0.01$ – 0.04 . These simulations show that $d\Gamma_n/d|n'|$ indeed changes sign along the boundary separating the L and H mode regimes in Fig. 1. This prediction is supported by a study of Alcator C-Mod edge parameters at the L - H transition [12].

Poloidal $\mathbf{E} \times \mathbf{B}$ shear flows, generated locally by the turbulence, lead in part to the large transport reduction with increasing α_d seen in Fig. 2(a). The ordering on which our model is based, however, excludes a contribution to the E_r shear that can arise from profile variations beyond the intrinsic turbulence scale. This possibly understates the importance of E_r shear since such profile shear will reinforce the stability of the system during the steepening process [6,7]. To address this issue, we carried out simulations of the edge pedestal in the context of a simple model. The model includes a source and sink (radially periodic) in the density equation (3), intended to represent neutral particle fueling in the edge. The strength of the source is chosen so that for $\alpha_d \sim 1$ and $\alpha \ll 1$ the source produces only a slight steepening of the profile before the system comes into equilibrium. We then slowly increase α with time. With increasing α the transport drops and the source causes the gradient to steepen, enhancing the turbulence until a new equilibrium is reached. At a critical value of α the region of maximum pressure gradient exceeds the L - H threshold condition and the profiles spontaneously begin to steepen. The subsequent evolution depends on the parameter ϵ_n : at $\epsilon_n = 0.02$ it is smooth, while at $\epsilon_n = 0.01$ it is bursty. Figure 4(a) shows the flux $\Gamma_{p_i}(t)$ from a simulation that includes the source in the latter case with $\alpha_d = 1$ and (initially) $\alpha = 0.05$. At $t = 1550$ the source is turned on and the value of α is slowly increased at a rate $d\alpha/dt = 2.5 \times 10^{-3}$. This causes the transport to drop gradually until $t = 1630$ ($\alpha \approx 0.25$), when a burst of turbulence produces a large $\mathbf{E} \times \mathbf{B}$ poloidal sheared flow. This can be seen in Fig. 4(b), which shows the time evolution of the root mean square poloidal $\mathbf{E} \times \mathbf{B}$ velocity \bar{v}_{E_y} (dotted line), ion diamagnetic velocity \bar{v}_{diy} (dashed line), and total ion rotation $\bar{v}_{iy} = \bar{v}_{E_y} + \bar{v}_{diy}$ (solid line). This $\mathbf{E} \times \mathbf{B}$ flow sharply reduces the flux and induces a localized transport barrier (much smaller than the box size), which in turn leads to a steepening of density profile that is reflected in a slow rise of the ion diamagnetic flow from 1650 to 1750. At $t = 1750$ ($\alpha \approx 0.5$) the barrier is disrupted by a large scale resistive ballooning mode which again produces strong $\mathbf{E} \times \mathbf{B}$ sheared flow [see Fig. 5(a), solid line] and suppression of the transport. A

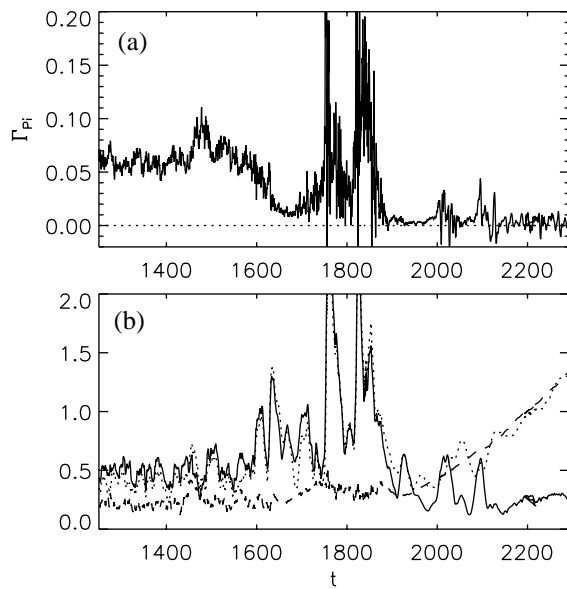


FIG. 4. (a) Γ_{p_i} vs t ; (b) \bar{v}_{iy} (solid line); \bar{v}_{diy} (dashed line); \bar{v}_{Ey} (dotted line).

similar event at $t \approx 1820$ leads finally to the formation of a global transport barrier at $t = 1920$. Beyond this, the diamagnetic velocity in Fig. 4(b) increases monotonically as the profiles continue to steepen, while the total ion flow slowly decays due to the effect of magnetic pumping. Since $v_{iy} = v_{Ey} + v_{diy} \approx 0$, this forces \bar{v}_{Ey} to increase in proportion to \bar{v}_{diy} , as seen in the figure. The growth of v_{Ey} , the radial profile of which is shown in Fig. 5(a) (dotted line) at a late time, reinforces the bifurcation of the system by suppressing turbulence in the pedestal everywhere except in a small region surrounding the maximum pressure gradient where $E'_r \approx 0$.

The steepening of the profiles following the transition is not limited by the ideal $n \rightarrow \infty$ MHD stability limit. This is shown in Fig. 5(b), which is a plot of the ion pressure profile at an early (dashed line) and late (solid line) time in a simulation with $\epsilon_n = 0.02$, $\alpha_d = 1$. The α value at the center of the pedestal, $\alpha(x=0) = 1.6$, is well beyond the first stability limit ($\alpha = 0.8$ at $\hat{s} = 1$). Long wavelength ideal modes with $k_y < 1/L_p$ are stable because the radial localization of the pedestal gradient greatly weakens the drive of such modes relative to the stabilizing contribution of magnetic line bending. Shorter wavelength modes with $k_y \gtrsim 1/L_p$ are stabilized by a combination of ω_{*i} and $\mathbf{E} \times \mathbf{B}$ shear effects.

In conclusion, while we expect the thresholds of Fig. 1 to depend on factors not discussed here, in particular,

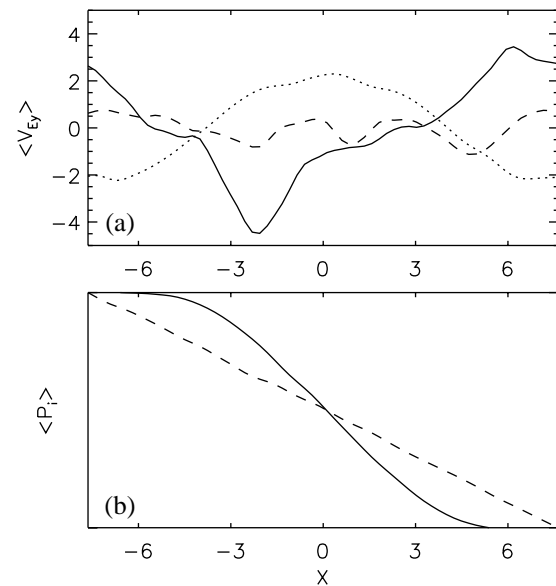


FIG. 5. (a) $\mathbf{E} \times \mathbf{B}$ flows before (dashed line), during (solid line), after (dotted line) transition; (b) early (dashed line), late (solid line) p_i profiles.

T_i/T_e , noncircular geometry, and \hat{s} , the framework on which they are based should be robust.

We acknowledge extensive discussions with T. Carlstrom, M. Greenwald, R. Groebner, A. Hubbard, R. Moyer, T. Osborne, W. Suttrop, and D. Thomas.

-
- [1] F. Wagner *et al.*, Phys. Rev. Lett. **49**, 1408 (1982).
 - [2] K. Burrell *et al.*, Phys. Fluids B **2**, 1405 (1990).
 - [3] M. Greenwald *et al.*, Nucl. Fusion **28**, 2199 (1988).
 - [4] B.N. Rogers and J.F. Drake, Phys. Rev. Lett. **79**, 229 (1997).
 - [5] B.D. Scott, Plasma Phys. Controlled Fusion **39**, 1635 (1997).
 - [6] K. Burrell *et al.*, *Plasma Physics and Controlled Fusion Research* (IAEA, Vienna, 1994), Vol. 1, p. 221.
 - [7] P.H. Diamond *et al.*, *Plasma Physics and Controlled Fusion Research* (Ref. [6]), paper D-2-II-6.
 - [8] A. Zeiler *et al.*, Phys. Plasmas **3**, 2951 (1996).
 - [9] W. Suttrop (private communication).
 - [10] J.F. Drake *et al.*, Phys. Rev. Lett. **75**, 4222 (1995).
 - [11] O. Pogutse *et al.*, in *Proceedings of the 24th European Physical Society Conference, Berchtesgaden, 1997* (European Physical Society, Petit-Lancy, 1997), Vol. 3, p. 1041.
 - [12] A. Hubbard *et al.*, Plasma Phys. Controlled Fusion **40**, 689 (1998).